NIMFEIA

Deliverable D2.4

Report on microwave antennas

Project Number	101070290
Project name	Nonlinear Magnons for Reservoir Computing in Reciprocal Space
Project acronym	NIMFEIA
Work Package	WP2
Type	Report
Dissemination level	Public
Lead Beneficiary	HZDR
Due date of delivery	Month 18 - March 2024

Author(s): Katrin Schultheiss (HZDR), Christopher Heins (HZDR), Attila Kákay (HZDR), Helmut Schultheiss (HZDR), Gerhard Jakob (JGU), Mathias Kläui (JGU), Fabian Kammerbauer (JGU)

Disclaimer:

The NIMFEIA project has received funding by the European Union's Research and Innovation Programme Horizon Europe under grant agreement No 101070290. However, views and opinions expressed in this document are those of the authors only and do not necessarily reflect those of the European Union. The European Union cannot be held responsible for them.

1. Summary

This report discusses excitation efficiencies of different microwave antennas, related to Milestone M3 *Implementation of microwave antennas facilitating scalability of the magnon reservoir* of Work Package 2 *Laboratory-scale experiments*. The operation principle of a magnon reservoir requires a strong excitation field for reaching the nonlinear regime. However, only a fraction of the rf-power, which is applied to the input microwave antenna, is actually absorbed by one individual magnon reservoir. Hence, one single microwave antenna can simultaneously feed multiple reservoirs as is corroborated by the experimental results shown in this report. Furthermore, the excitation efficiency of different antenna designs are compared.

2. Differences in the antenna designs

Our previous experiments demonstrating the working principle of the magnon scattering reservoir relied on the out-of-plane excitation of a single reservoir inside an Ω-shaped antenna [1]. However, this approach allowed us to address only one reservoir at a time. Moving to a different reservoir required contacting a different antenna. Therefore, we designed various antennas to explore their potential and scalability for addressing several magnon reservoirs via one single rf input. Figure 1 shows exemplary scanning electron microscope (SEM) images of two antennas, with the bright contrast resembling the Au antenna structures on the black background of the Si substrate. Both designs rely on a coplanar waveguide (CPW) geometry with a central signal line (S) surrounded on both sides by shielding ground lines (G). These on-chip CPWs can be connected to microwave sources using rf contact needles. The magnon reservoirs (dark grey contrast) are positioned in the central part of the CPW, as can be seen better from the close-ups in Figs. 1 (c), (d). There, one can also see the differences in the working principles of two antenna types. Relying on our experience, Fig. 1 (c) shows the well-known Ω-shaped short of the CPW, with the disk-shaped reservoir in its center. Inside the Ω loop, microwave currents flowing through the antenna provide oscillating out-of-plane magnetic Oersted fields strong enough to excite nonlinear dynamics in the magnon reservoir. However, this limits the simultaneous excitation to maximal two reservoirs. The second approach shown in Figs. 1 (b), (d) relies on a continuous CPW for microwave transduction to a second rf contact needle which is connected to a 50 Ω termination. This antenna design brings two advantages: First, the reservoirs can be excited by out-of-plane or in-plane oscillating magnetic fields depending on their positioning, either in between the signal and ground lines or on top of the signal line. Second, many different magnon reservoirs can be placed next to each other along the signal line of the CPW.

To fabricate the samples discussed in this report, we employed a three step process: First, on a 1 x 1 cm^2 Si chip, we patterned the macroscopic CPW parts for 45 devices using an optical mask and UV lithography, electron beam evaporation of a Cr(5nm)/Au(50nm) film and lift-off. In a second step, in 200 x 200 μm^2 areas in the center of each device, we define individual antenna designs using electron beam lithography, electron beam evaporation of a Cr(5nm)/Au(65nm) film and lift-off. In the last step, we pattern the magnon reservoirs in between or on

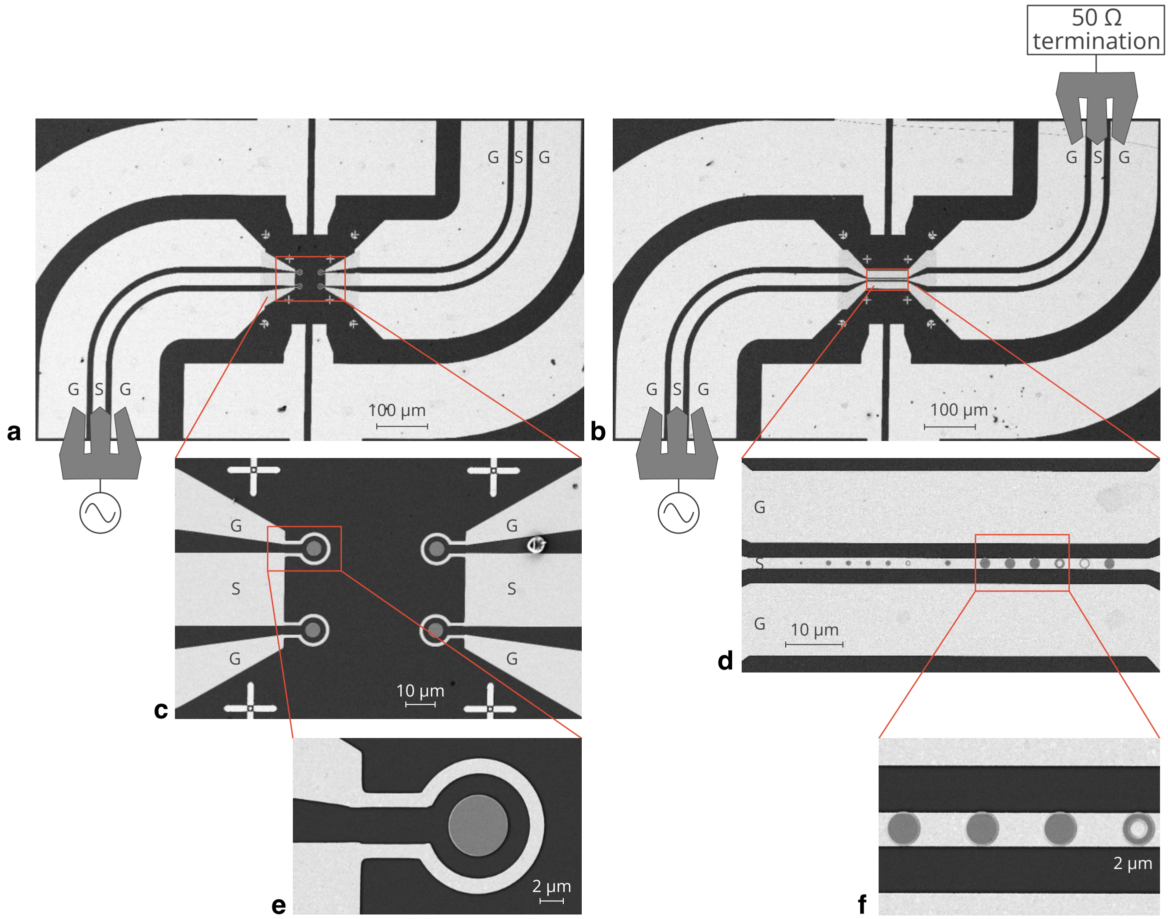

Figure 1: Scanning electron microscope (SEM) images of different antenna designs. The bright areas show Au structures on the black background of the Si substrate. (a),(b) Both antennas are based on a coplanar waveguide (CPW) geometry which consists of a central signal line (S) in between two shielding ground lines (G). The CPWs are connected to a microwave source using rf contact needles. (a) Shorted CPW with an Ω-shaped antenna placed in the short. (b) Continuous CPW for microwave transduction to a second rf needle which is connected to a 50 Ω termination. (c),(d) Close ups of the antennas where the magnon reservoirs (gray disks) are positioned. (c) The Ω-shaped shorts of the CPW provide oscillating out-of-plane magnetic fields for exciting reservoirs positioned in their center. (d) The continuous CPW provides in-plane (out-of-plane) excitation fields for reservoirs positioned on top of the signal line (in between signal and ground line), respectively. (e) Close-up of a 5-µm wide, disk-shaped magnon reservoir positioned in the center of one of the Ω-shaped shorts. (f) Close-up of 2-µm wide, disk-shaped magnon reservoirs positioned on the signal line of a CPW.

top of the Au structures, again, using electron beam lithography, magnetron sputtering of a $Ni_{47}Cr_{42}Fe_{11}$(4nm)/$Ni_{81}Fe_{19}$(50nm)/Ta(4nm) film in a rotating magnetic field (for details of the material parameters see Deliverable D4.1 *Report on soft metallic systems*) and lift-off. This way, on a single chip, we fabricate 45 devices with varying antennas and magnon reservoirs for direct comparison independent of any chip-to-chip variations in the material parameters.

3. Comparing excitation efficiencies

In this study, we focus on disk-shaped magnon reservoirs with two different diameters of 2 µm and 5 µm. To evaluate the excitation efficiencies of different antennas, we used Brillouin light scattering microscopy. Therefore, a continuous-wave, monochromatic 532-nm laser was fo-

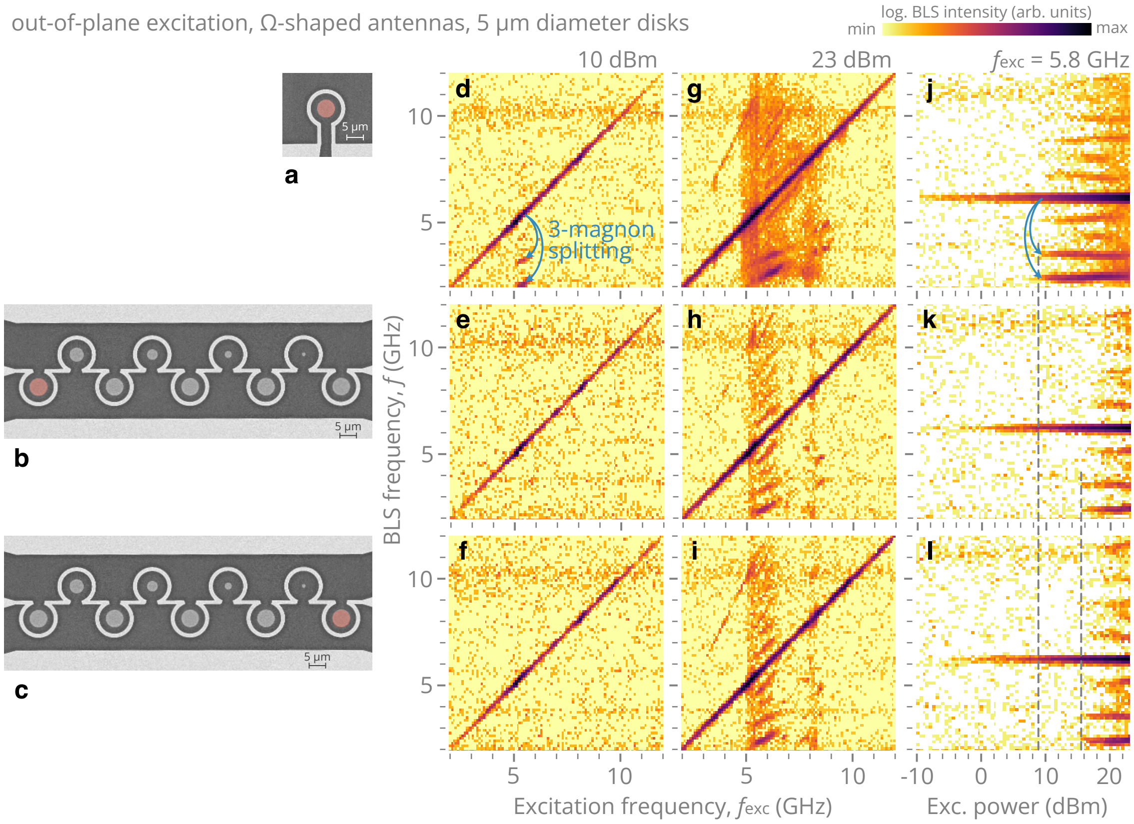

Figure 2: Comparison of different Ω-shaped antennas for out-of-plane excitation. (a)-(c) SEM images of the studied antennas with the investigated 5 µm-wide, disk-shaped magnon reservoirs highlighted in red. (d)-(i) BLS spectra measured for different excitation frequencies at excitation powers of (d)-(f) 10 dBm and (g)-(i) 23 dBm. (j)-(l) BLS spectra recorded as a function of excitation power for an excitation frequency of 5.8 GHz. The detected BLS intensities are color coded on a logarithmic scale.

cused onto the surface of the magnon reservoir using a microscope lens with a high numerical aperture, yielding a spatial resolution of about 300 nm. The backscattered light was then directed into a Tandem Fabry-Pérot interferometer to measure the frequency shift caused by the inelastic scattering of photons and magnons. The detected intensity of the frequency-shifted signal is directly proportional to the magnon intensity at the respective focusing position. To account for different spatial distributions of the nonlinearly excited magnons, the signals were integrated over 12 positions across half the disk.

We begin by comparing 5 µm-wide magnon reservoirs that are excited by out-of-plane magnetic fields using different Ω-shaped antennas, shown by SEM images in Fig. 2(a)-(c). The respective studied reservoir is highlighted in red. In general, we compare two different types of measurements: First, we plot BLS spectra measured as a function of the excitation frequency f_{exc} for a fixed excitation power, e.g. Fig. 2(d). The detected BLS intensities are color coded on a logarithmic scale. Here, any nonlinear response of the reservoir manifests in the detection of off-diagonal signals. The most prominent nonlinear process is the three-magnon scattering, where the directly excited mode f_{exc} splits in two secondary modes $f_+ = f_{\mathrm{exc}}/2 + \delta f$ and $f_- = f_{\mathrm{exc}}/2 - \delta f$ under the conservation of energy and angular momentum. Second, we select one prominent excitation frequency for which we measured nonlinear three-magnon splitting and sweep its excitation power, e.g. Fig. 2(j). Again, the detected BLS intensities are color cod-

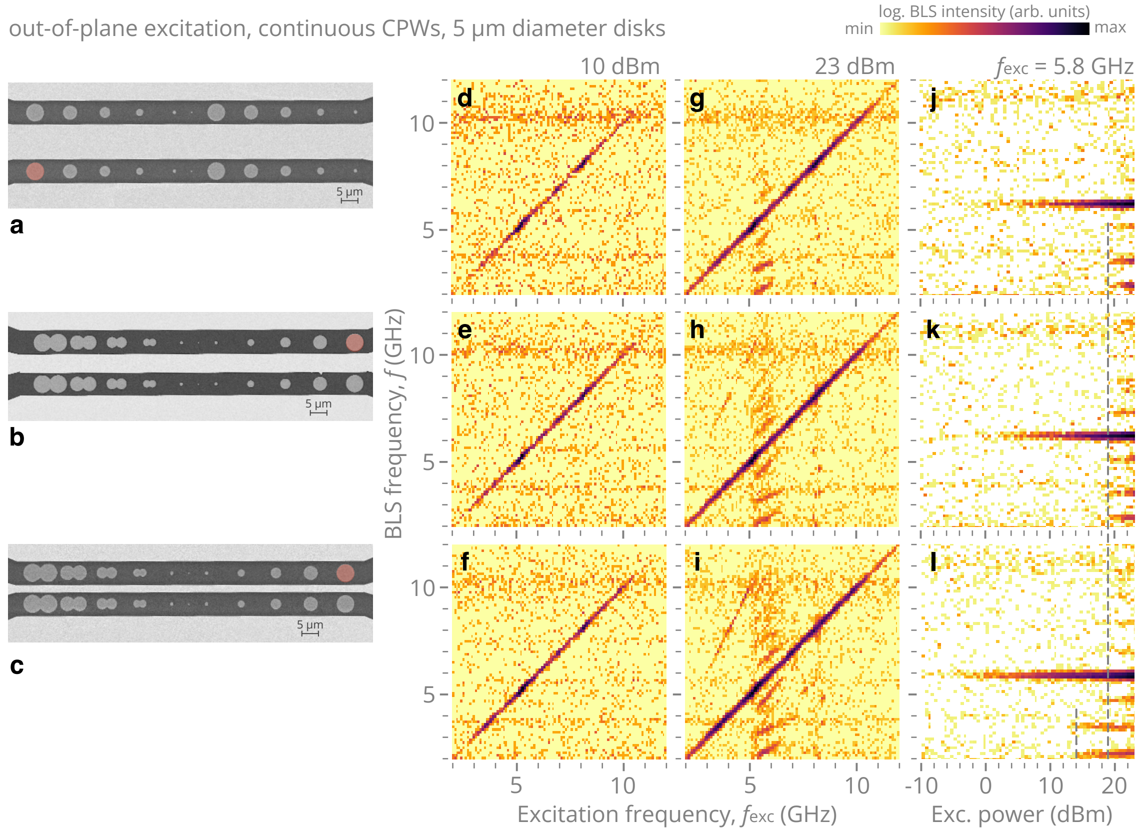

Figure 3: Comparison of continuous CPW antennas with varying signal line widths for out-of-plane excitation. (a)-(c) SEM images of the studied antennas with the investigated 5 µm-wide, disk-shaped magnon reservoirs highlighted in red. (d)-(i) BLS spectra measured as a function of excitation frequency at excitation powers of (d)-(f) 10 dBm and (g)-(i) 23 dBm. (j)-(l) BLS spectra recorded as a function of excitation power for an excitation frequency of 5.8 GHz. The detected BLS intensities are color coded on a logarithmic scale.

ed. Thereby, we can directly compare the threshold powers for nonlinear magnon scattering using different antennas. The top line in Fig. 2 shows the results for the known individual Ω-shaped antenna at the CPW's short. The middle (bottom) line presents the results for a chain of Ω-antennas measured on the most left (right) reservoir, respectively.

At the lower excitation power of 10 dBm, only the individual Ω-shaped short shows slight nonlinearity. At the higher power of 23 dBm, all three investigated reservoirs operate in the nonlinear regime. When exciting the reservoirs at f_{exc} = 5.8 GHz, the power threshold for the Ω-shaped short lies around 9 dBm whereas it is just below 16 dBm for the chained Ω-antennas. This shows that despite the reduced efficiency, the rf transmission through the chain of Ω-antennas is still sufficient to reach the operating regime of the magnon reservoir. Remarkably, there is no difference between the left and right reservoir, demonstrating that all nine reservoirs in the chain can be operated simultaneously, which can be scaled up to several orders of magnitude higher numbers. The increase in the threshold microwave power will be compensated later in the project by using magnetic materials with lower magnetic damping.

In a next step, we keep the out-of-plane excitation but use a different antenna design. As shown in Figs. 3(a)-(c), the 5 µm-wide magnon reservoirs are positioned in between the signal and ground line of a continuous CPW antenna. The width of the signal line reduces from 10

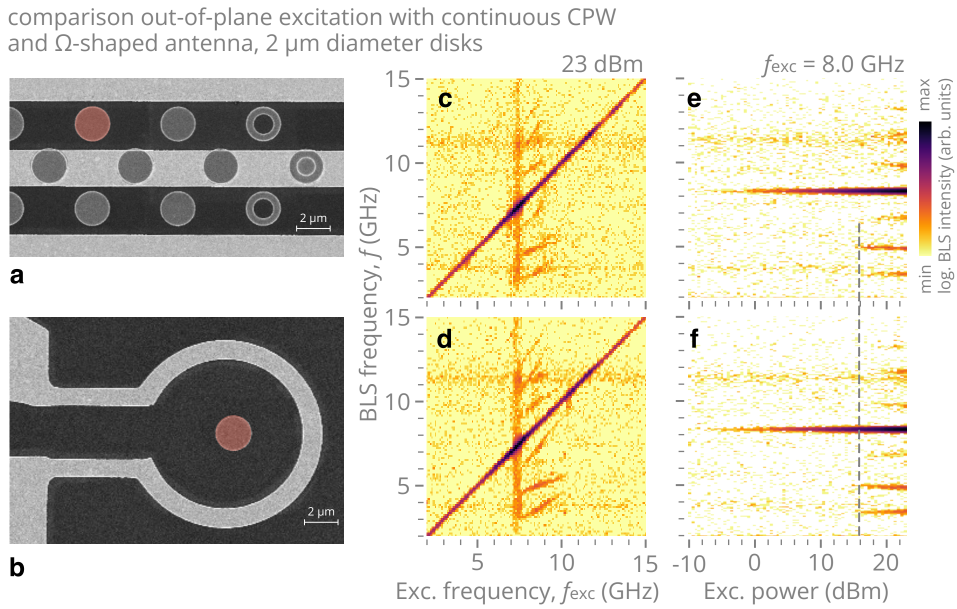

Figure 4: Comparison of the out-of-plane excitation efficiency using a continuous CPW and an Ω-shaped antenna. (a),(b) SEM images of the studied antennas with the investigated 2-µm wide, disk-shaped magnon reservoirs highlighted in red. (c),(d) BLS spectra measured as a function of excitation frequency at an excitation power of 23 dBm. (e),(f) BLS spectra recorded as a function of excitation power for an excitation frequency of 8.0 GHz. The detected BLS intensities are color coded on a logarithmic scale.

µm (top line in Fig. 3) over 5 µm (middle line) to 2 µm only (bottom line). The respective studied reservoir is highlighted in red in the SEM images. While the lower excitation power of 10 dBm does not show a nonlinear response in any of the reservoirs, three-magnon splitting is observed for all antennas at the higher power of 23 dBm. The narrower the CPW's signal line, the more efficient the excitation. This was expected since the same current amplitude is forced through a narrower signal line resulting in a stronger magnetic Oersted field. For the 2 µm-wide signal line, the power threshold is about 14 dBm, very similar to the chain of Ω-shaped antennas in Figs. 2(k), (l). For the wider signal lines, the efficiency decreases and a higher power of about 19 dBm is required to reach the nonlinear operating regime of the reservoir. Nonetheless, this approach offers the chance to position multiple reservoirs of different shapes next to each other and address all of them using a single microwave antenna.

To corroborate the usefulness of continuous CPW antennas, we test the two different out-of-plane excitation schemes on a vortex-based reservoir with another dimension. In Fig. 4, we compare measurements on 2 µm-wide disk-shaped reservoirs, one positioned in between the signal and ground line of a continuous CPW (top line), the other positioned inside an Ω-shaped short (bottom line). Interestingly, the BLS spectra measured as a function of the excitation frequency show similar magnon intensities in the nonlinear regime and there is no difference in the threshold powers which is about 16 dBm at an excitation frequency of 8 GHz. Note that due to the reduced dimension of the reservoir, the frequencies for which we measure a nonlinear response are higher compared to 5 µm-wide reservoirs. Nonetheless, the power thresholds to reach the nonlinear regime are similar in both reservoir sizes.

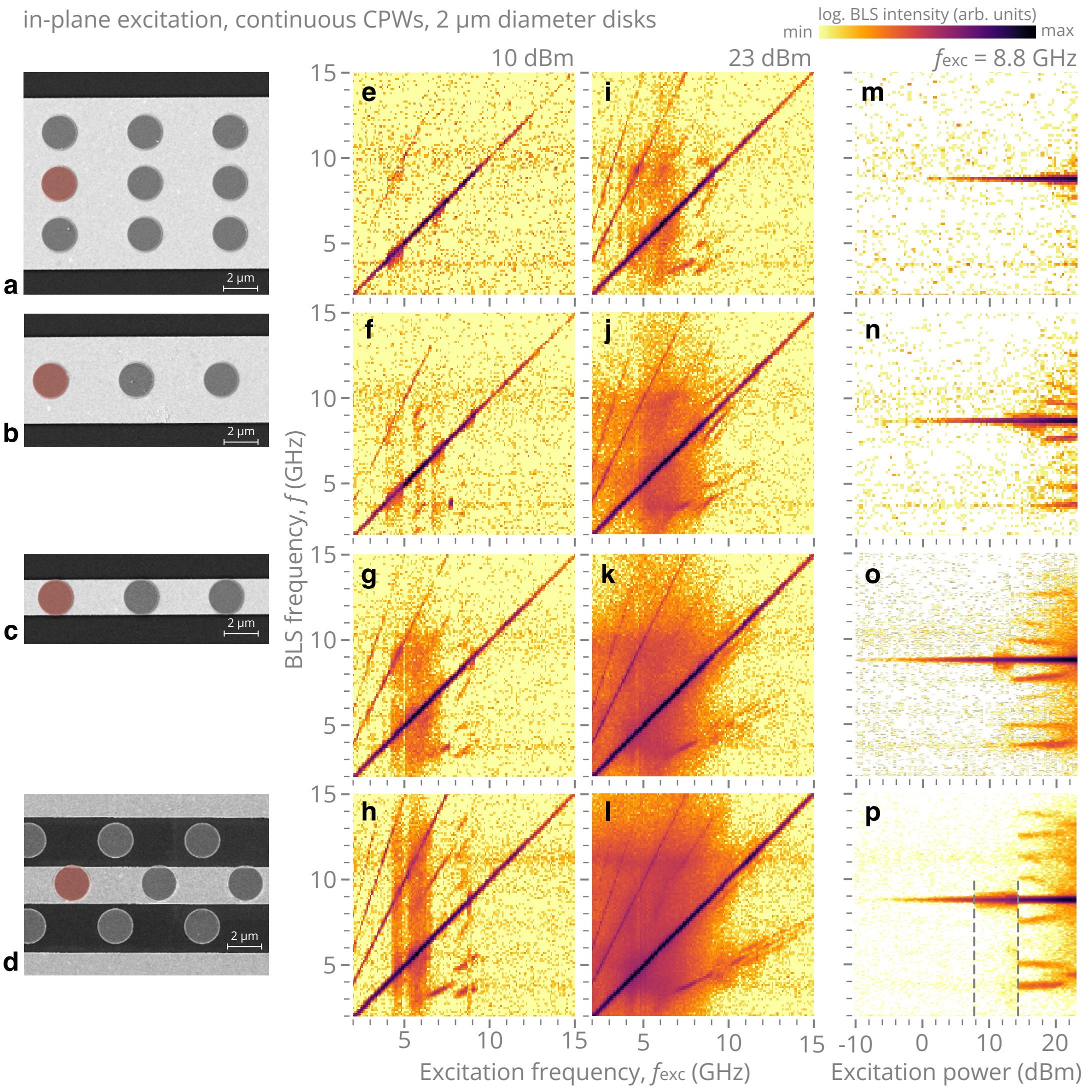

Figure 5: Comparison of the in-plane excitation efficiency using continuous CPW antennas with varying signal line widths. (a)-(d) SEM images of the studied antennas with the investigated 2-µm wide, disk-shaped magnon reservoirs highlighted in red. (e)-(l) BLS spectra measured as a function of excitation frequency at excitation powers of (e)-(h) 10 dBm and (i)-(l) 23 dBm. (m)-(p) BLS spectra recorded as a function of excitation power for an excitation frequency of 8.8 GHz. The detected BLS intensities are color coded on a logarithmic scale.

As already mentioned, one major advantage of continuous CPW antennas lies in their flexibility. In addition to the out-of-plane excitation discussed so far, we can harness the oscillating in-plane magnetic Oersted fields as well by simply positioning the magnon reservoirs on top of the signal line. Figure 5 compares the in-plane excitation efficiencies of continuous CPWs with varying widths of their signal lines from 10 µm (top line) over 5 µm (second line) to 2 µm (third and bottom line). In general, one can see that the nonlinear response – visible in the off-diagonal signals – is much stronger with the in-plane excitation compared to the out-of-plane excitations discussed before. Even at an excitation power of 10 dBm, all antennas show a nonlinear response, the 10 µm-wide antenna quite weakly though. Additionally, the narrower the signal line, the stronger the nonlinearity. As already mentioned above, this can be attributed to forcing the same current amplitude through a narrower antenna which results in the generation of stronger magnetic Oersted fields.

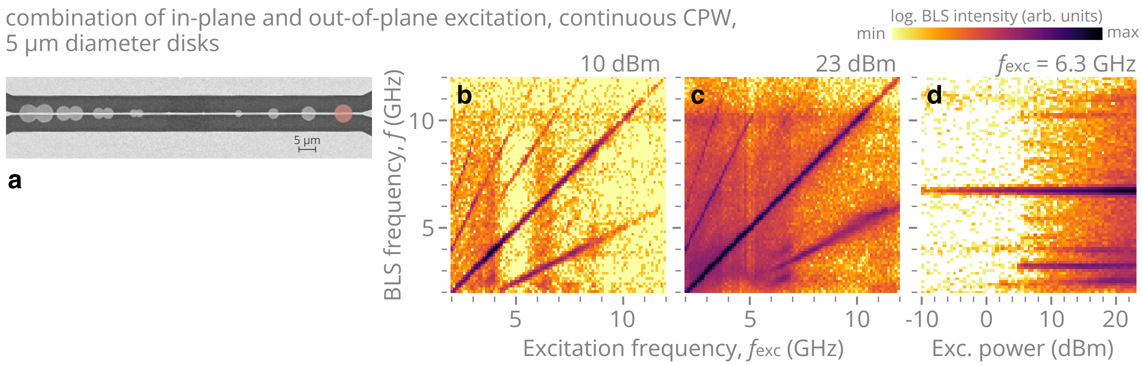

Figure 6: Combination of in-plane and out-of-plane excitation using a continuous CPW with a 500 nm-wide signal line. (a) SEM image of the studied structure. The studied 5 µm-wide, disk-shaped reservoir is highlighted in red. (b),(c) BLS spectra measured for different excitation frequencies at excitation powers of (b) 10 dBm and (c) 23 dBm. (d) BLS spectra recorded for a fixed excitation frequency of 6.3 GHz at increasing excitation powers. Exceeding the threshold of 5 dBm nonlinear dynamics set in. The detected BLS intensity is color coded on a logarithmic scale.

In the BLS spectra measured at 10 dBm [Fig. 5(e)-(h)], some excitation frequencies lead to a significant line broadening of the measured BLS frequencies. At 23 dBm and for the narrower signal lines, this becomes even more pronounced and is visible almost over the entire range of excitation frequencies [Fig. 5(k),(l)]. We attribute this to the generation of Floquet magnon bands which manifest themselves in the measurement of frequency combs, both around the direct excitation and the nonlinear split modes. The spacing of these frequency combs is determined by the resonance frequency of the gyrotropic vortex mode, which is around 200 MHz in a 2 µm-wide and 50 nm-thick $Ni_{81}Fe_{19}$ disk and cannot be resolved in the BLS spectra. Hence the prominent broadening of the magnon frequencies. Depending on the disk size, the threshold for the generation of these Floquet magnon bands can be lower or higher compared to the threshold for three-magnon splitting. For an excitation frequency of 8.8 GHz on a 2 µm-wide signal line [Fig. 5(p)], for example, we measure a broadening of the direct excitation already starting at 8 dBm. For excitation powers above 14 dBm, very abruptly, we detect clear signals of three-magnon splitting. This indicates a sharp shift between the different nonlinear regimes. Note that at excitation powers around 20 dBm, we measure a transition from three-magnon splitting $f_{\mathrm{exc}} \rightarrow f_{\pm} = f_{\mathrm{exc}}/2 \pm \delta f$ to splitting into half the excitation frequency $f_{\mathrm{exc}} \rightarrow f_{\pm} = f_{\mathrm{exc}}/2$ with degenerate split modes $f_{+} = f_{-}$, which can be attributed to parallel pumping.

The third and bottom line in Fig. 5 essentially compare the same antenna design with 2 µm-wide signal lines. Nevertheless, we wanted to make the point that despite the fact that the antenna in Fig. 5(d) hosts many more magnon reservoirs, the thresholds for reaching the nonlinear regime are the same. This demonstrates that even though high powers are required to reach nonlinearity, one reservoir hardly absorbs any energy so that many reservoirs can be operated simultaneously using the same antenna.

The last antenna design in Fig. 6 combines both excitation regimes. By reducing the width of the CPW's signal line to 500 nm and placing it across the reservoirs' centers, both out-of-plane and in-plane magnetic Oersted fields couple to the magnetization inside the magnon reservoir. Interestingly, at an excitation power of 10 dBm, parallel pumping into half the excitation frequency seems to dominate. Only at a higher excitation power of 23 dBm, three-magnon splitting is measured.

4. Conclusion

Overall, we have demonstrated that the design of continuous coplanar waveguide antennas allows for the efficient excitation of magnon reservoirs using either in-plane or out-of-plane magnetic Oersted fields. Placing several reservoirs on a single CPW antenna did not change the thresholds for reaching the nonlinear operation regime. This facilitates the simultaneous operation of a large number of reservoirs, the upper limits of which have yet to be tested. Additionally, using in-plane excitation allows us to directly tackle the vortex gyration, an eigenmode of the vortex state disk with frequencies in the range of a few hundred MHz. This opens up possibilities for reducing the operating frequencies of the vortex-based magnon reservoirs from the lower GHz to the higher MHz range or even for multi-tone operation.

5. References

[1] L. Körber, C. Heins, T. Hula, J.-V. Kim, S. Thlang, H. Schultheiss, J. Fassbender, K. Schultheiss. Pattern recognition with a magnon-scattering reservoir. *Nature Communications* 14, 3954 (2023)